Pramana – J. Phys. (2017) 89:89
https://doi.org/10.1007/s12043-017-1486-9

First-principle calculations of structural, electronic, optical, elastic and thermal properties of $MgXAs_2$ (X = Si, Ge) compounds

S CHEDDADI[1], K BOUBENDIRA[1], H MERADJI[1,*], S GHEMID[1], F EL HAJ HASSAN[2], S LAKEL[3] and R KHENATA[4]

[1]Laboratoire de Physique des Rayonnements, Département de Physique, Faculté des Sciences, Université Badji Mokhtar, Annaba, Algeria
[2]Laboratoire de Physique et d'électronique (LPE), Faculté des Sciences I, Université Libanaise, El Hadath, Beirut, Lebanon
[3]Laboratoire des Matériaux Semi-Conducteurs et Métalliques, Université de Biskra, Biskra, Algeria
[4]Laboratoire de Physique Quantique de la Matière et de la Modélisation Mathématique (LPQ3M), Université de Mascara, 29000 Mascara, Algeria
*Corresponding author. E-mail: hmeradji@yahoo.fr

MS received 17 May 2017; revised 31 July 2017; accepted 2 August 2017; published online 28 November 2017

Abstract. First-principle calculations on the structural, electronic, optical, elastic and thermal properties of the chalcopyrite $MgXAs_2$ (X = Si, Ge) have been performed within the density functional theory (DFT) using the full-potential linearized augmented plane wave (FP-LAPW) method. The obtained equilibrium structural parameters are in good agreement with the available experimental data and theoretical results. The calculated band structures reveal a direct energy band gap for the interested compounds. The predicted band gaps using the modified Becke–Johnson (mBJ) exchange approximation are in fairly good agreement with the experimental data. The optical constants such as the dielectric function, refractive index, and the extinction coefficient are calculated and analysed. The independent elastic parameters namely, C_{11}, C_{12}, C_{13}, C_{33}, C_{44} and C_{66} are evaluated. The effects of temperature and pressure on some macroscopic properties of $MgSiAs_2$ and $MgGeAs_2$ are predicted using the quasiharmonic Debye model in which the lattice vibrations are taken into account.

Keywords. Chalcopyrites; first-principle calculations; electronic properties; thermal properties; band gap; optical properties.

PACS Nos **71.15.Ap; 71.15.Mb; 71.15.Nc; 71.20.Nr; 65.40.Ba; 65.40.De; 78.20.Ci**

1. Introduction

II–IV–V_2 chalcopyrite semiconductors generally crystallize in tetragonal structure with the space group $I\bar{4}2d(D_{2D}^{12})$. These compounds attracted considerable attention due to their photovoltaic characteristics. Chalcopyrites are promising materials for spintronics, electronic and optoelectronic applications such as solar energy converters, infrared detectors, visible and invisible light emitting diodes [1–4]. $MgXAs_2$ (X = Si, Ge) compounds are synthesized in chalcopyrite phase [1,5]. Shaposhnikov *et al* [6] investigated the electronic and the optical properties of $MgSiAs_2$ and $MgGeAs_2$ compounds. Liwei and coworkers [7] performed *ab-initio* band structure calculations for $MgSiAs_2$ compound. The authors [6,7] have found that both $MgSiAs_2$ and $MgGeAs_2$ are direct band-gap semiconductors. Basalaev and Demushin [8] studied the electronic band structure and the chemical bonding properties of the chalcopyrite $MgBX_2$ (B = Si, Ge, Sn; X = As, P, Sb) compounds and the orthorhombic $MgYN_2$ (Si, Ge) compounds. Kocak and Ciftci [9] investigated the elastic and the optical properties of $MgGeAs_2$ whereas Boukabrine *et al* [10] studied the dielectric function of $MgXAs_2$ (X = Si, Ge).

In the present work, we have focussed on the study of the structural, electronic, optical, elastic and thermal properties of $MgXAs_2$ (X = Si, Ge) compounds in their chalcopyrite phase. The computed ground-state structural properties have been compared with the available experimental and theoretical data. The outline of the paper is as follows: In §2 we give a brief description

of computational details adopted for the calculations. The calculations of the structural, electronic and optical properties along with the computed elastic and thermal properties are described in §3. Summary and conclusions are drawn in §4.

2. Method of calculation

The calculations reported here were done using the full-potential linearized augmented plane wave method (FP-LAPW) [11] within the framework of the density functional theory (DFT) [12,13], as implemented in the WIEN2K code [14]. The FP-LAPW method expands the Kohn–Sham orbitals as atomic-like orbitals inside the muffin-tin (MT) atomic spheres and plane waves in the interstitial regions. The Kohn–Sham equations were solved using the recently developed Wu–Cohen generalized gradient approximation (WC-GGA) [15] for the exchange-correlation (XC) potential. Furthermore, the modified Becke–Johnson potential (mBJ) [16] coupled with WC-GGA is used for the computation of electronic properties. The valence wave functions inside the atomic spheres were expanded up to $l = 10$ partial waves. In the interstitial regions, a plan-wave expansion with $R_{\mathrm{MT}}K_{\max} = 7$ was used for all the investigated systems, where R_{MT} is the minimum radius of the muffin-tin spheres and $K_{\max}$ gives the magnitude of the largest K vector in the plane-wave expansion. The potential and the charge density were Fourier expanded up to $G_{\max} = 12(\mathrm{Ryd})^{1/2}$. R_{MT} (muffin-tin radii) are taken to be 2.21, 2.0, 2.18 and 2.0 atomic units (a.u.) for Mg, Si, Ge and As, respectively. The modified tetrahedron method [17] was applied to integrate inside the Brillouin zone (BZ) with a dense mesh of 5000 uniformly distributed k-points (equivalent to 405 in irreducible BZ) where the total energy converges to less than 10^{-6} Ry.

3. Results and discussion

3.1 *Structural properties*

At ambient condition, II–IV–V_2 ternary compounds crystallize in the body centred tetragonal (BCT) chalcopyrite structure belonging to the space group $I\bar{4}2d$ (N^o : 122). As shown in figure 1, the chalcopyrite structure is closely related to the zinc blende structure and contains four formula units in each unit cell, with the II, IV and V atoms occupying Wyckoff positions 4*a* (0, 0, 0), 4*c* (0, 0, 0.5) and 8*d* (*u*, 0.25, 0.125), respectively, where *u* is the anion displacement parameter. In this structure, each II and IV cation is surrounded by four V anions, and each V anion is surrounded by two II and two IV cations. Generally, the chalcopyrite lattice is characterized by three structural parameters: the lattice constants *a* and *c*, as well as the dimensionless anion displacement parameter *u* determined by the following expression:

$$u = 0.25 + (d^2_{\mathrm{Mg-As}} - d^2_{\mathrm{X-As}}), \quad \mathrm{X} = \mathrm{Si},\ \mathrm{Ge}, \tag{1}$$

where $d_{\mathrm{Mg-As}}$ and $d_{\mathrm{X-As}}$ are the bond lengths between atoms of the corresponding groups. In an ideal chalcopyrite structure, $c/a = 2$ and $u = 0.25$. The larger the parameters c/a and u deviate from the ideal values, the higher is the degree of tetragonal distortion.

In our calculations, we have calculated the energy at different volumes, keeping c/a constant. The c/a ratio is optimized by calculating c/a vs. energy, keeping the volume fixed at its minimal value. The parameter

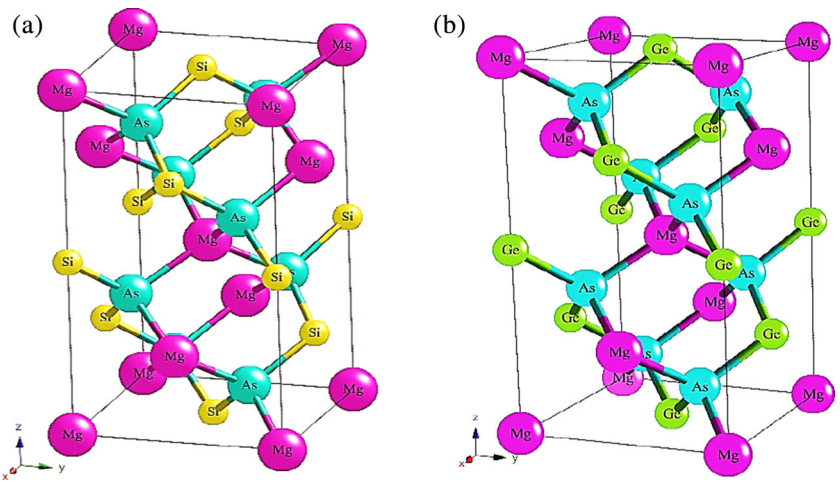

Figure 1. The crystal structure of chalcopyrite compounds: (**a**) $MgSiAs_2$ and (**b**) $MgGeAs_2$.

Table 1. Calculated structural equilibrium parameters, (a, c, u), bulk modulus (B) and the pressure derivative of the bulk modulus (B') of $MgSiAs_2$ and $MgGeAs_2$ using WC-GGA scheme.

Compounds	a (Å)	c (Å)	u	d_{Mg-As}	d_{X-As}	d_{Mg-X}	B (GPa)	B'
$MgSiAs_2$	5.874[a]	10.847[a]	0.287[a]	2.617[a]	2.356[a]	4.154[a]	63.12[a]	4.24[a]
	5.94[b]	10.59[b]	0.286[b]				63.109[b]	4.19[b]
	5.954[c]	10.80[c]	0.286[c]	2.633[c]	2.38[c]	4.019[c]		
$MgGeAs_2$	5.99[a]	11.03[a]	0.276[a]	2.622[a]	2.438[a]	4.236[a]	58.253[a]	4.4[a]
	6.009[b]	11.27[b]	0.273[b]					
	5.841[c]	11.068[c]	0.274[c]	2.632[c]	2.471[c]	4.119[c]		

[a]This work.
[b]Ref. [9].
[c]Ref. [6].

u is minimized by calculating the internal forces acting on the atoms within the unit cell until the forces become negligible by using the MINI program included in the WIEN2K code. The minimization of the total energy as a function of the unit cell volume is obtained using Murnaghan's equation of state [18]. The calculated equilibrium structural parameters (a, c and u), bulk modulus B and its pressure derivative B' together with the available theoretical data are listed in table 1. The calculated total energies vs. volumes of the $MgSiAs_2$, and $MgGeAs_2$ crystals are plotted in figure 2. The lattice constants, c/a ratio and u are found to be in close agreement with the previous theoretical results. The lattice constants increase as we move from Si to Ge whereas c/a, u and B decrease.

3.2 *Electronic properties*

The electronic properties of $MgSiAs_2$ and $MgGeAs_2$ compounds are obtained by calculating the band structures. The calculated band structures of the compounds along the high symmetry lines of the first Brillouin zone using both WC-GGA and mBJ schemes are shown in figure 3. The band structures of the considered compounds are almost similar with some difference in details such as bandwidth and the relative energies. It can be seen that the valence band maximum and the conduction band minimum are positioned at the Γ point, and so these compounds are direct band-gap materials; therefore they are interesting for the optoelectronic devices.

The band gaps determined using WC-GGA and mBJ schemes together with other theoretical and experimental results are given in table 2. From table 2, it is seen that the mBJ approximation gives results which are in good agreement with experimental values that are similar to those produced by more sophisticated methods, but at much lower computational cost [16,21]. One can remark also that our computed band-gap values are in good agreement with those obtained by other theoretical methods. The band gap decreases when Si is replaced by Ge.

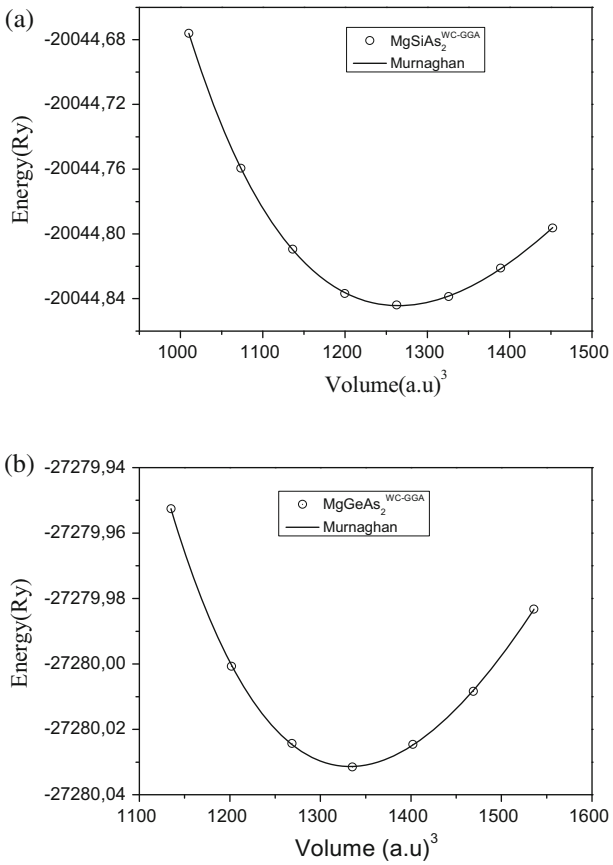

Figure 2. Calculated total energies of (**a**) $MgSiAs_2$ and (**b**) $MgGeAs_2$.

3.3 *Optical properties*

Optical properties of a solid are usually described in terms of the complex dielectric function $\varepsilon(\omega) = \varepsilon_1(\omega) + i\varepsilon_2(\omega)$ which is related to the interaction of photons and

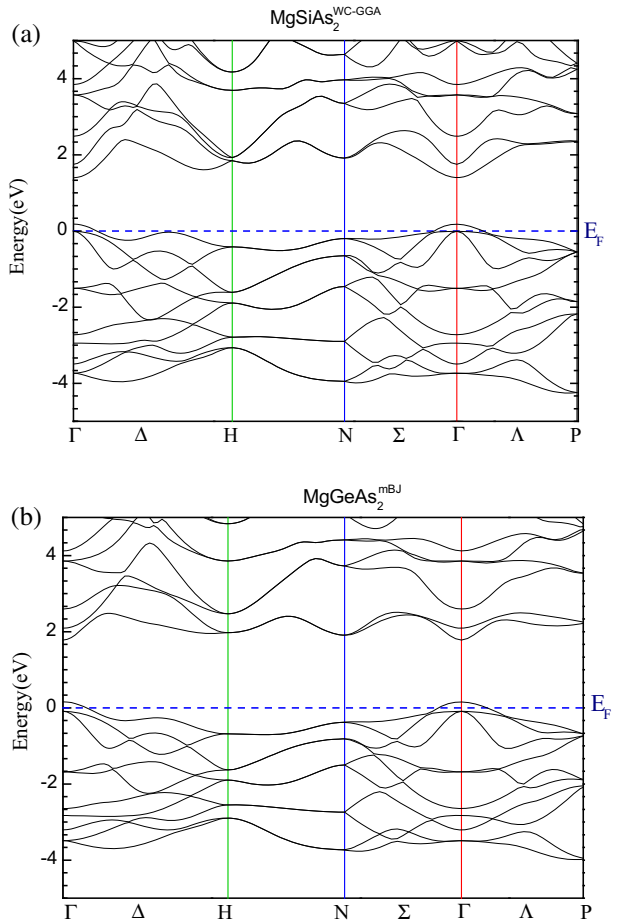

Figure 3. Calculated band structures of (**a**) $MgSiAs_2$ and (**b**) $MgGeAs_2$ using WC-GGA and mBJ, respectively.

electrons. The imaginary part of the dielectric function in the long wavelength limit has been obtained directly from the electronic structure calculation, using the joint density of states and the optical matrix elements. The real part of the dielectric function can be evaluated from the imaginary part by the Kramers–Kronig relation. The knowledge of both real and the imaginary parts of the dielectric function allows the calculation of other important optical functions such as the refractive index $n(\omega)$ and the extinction coefficient $k(\omega)$ given by the following relations:

$$n(\omega) = \left[\frac{\varepsilon_1}{2} + \frac{\sqrt{\varepsilon_1^2(\omega) + \varepsilon_2^2(\omega)}}{2}\right]^{1/2} \tag{2}$$

$$k(\omega) = \left[\frac{\sqrt{\varepsilon_1^2(\omega) + \varepsilon_2^2(\omega)}}{2} - \frac{\varepsilon_1}{2}\right]^{1/2}. \tag{3}$$

At low frequency ($\omega = 0$), we get the following relations:

$$n = \sqrt{\varepsilon_1} \tag{4}$$

$$k = \frac{\varepsilon_2}{2n}. \tag{5}$$

For tetragonal crystal systems, we need two tensor components (parallel and perpendicular to c-axis corresponding to the electric field) to complete the description of optical properties.

Figure 4 shows the calculated real part of the dielectric function $\varepsilon_1(\omega)$ for $MgSiAs_2$ and $MgGeAs_2$ compounds for the energy range 0–14 eV. It is evident from figure 4 that for both the investigated compounds, $\varepsilon_1(\omega)$ increases with increasing energy and reaches a maximum value at around 2.25 eV for $MgSiAs_2$ and 1.62 eV for $MgGeAs_2$, then it decreases to reach a negative minimum value at around 4.28 eV for $MgSiAs_2$ and 4.09 eV for $MgGeAs_2$. The negative values of $\varepsilon_1(\omega)$ show that in this energy region, the compound exhibits metallic characteristics. With further increase in energy, $\varepsilon_1(\omega)$ increases and shows steady behaviour for both materials at high energy limits. So the materials will be transparent for high-energy incident photons. Optical spectra exhibit anisotropy in two directions (along basal-plane and z-axis) with a very small difference (0.53 and 0.59 for $MgSiAs_2$ and $MgGeAs_2$, respectively) in the static limit. From Ge to Si the peaks decrease and shift towards the low-energy region.

Table 2. Calculated band-gap energy of $MgSiAs_2$ and $MgGeAs_2$.

	E_g (eV)			
	This work			
	WC-GGA	mBJ	Exp.	Other calculations
$MgSiAs_2$	1.217	1.970	2.00[a], 2.08[d]	1.22[b, PBE−GGA], 1.26[c, PBE−GGA], 1.95[c, mBJ]
$MgGeAs_2$	0.624	1.620	1.60[a, d]	0.57[c, PBE−GGA], 0.84[b, PBE−GGA], 1.39[c, mBJ]

[a]Ref. [19].
[b]Ref. [1].
[c]Ref. [6].
[d]Ref. [20].

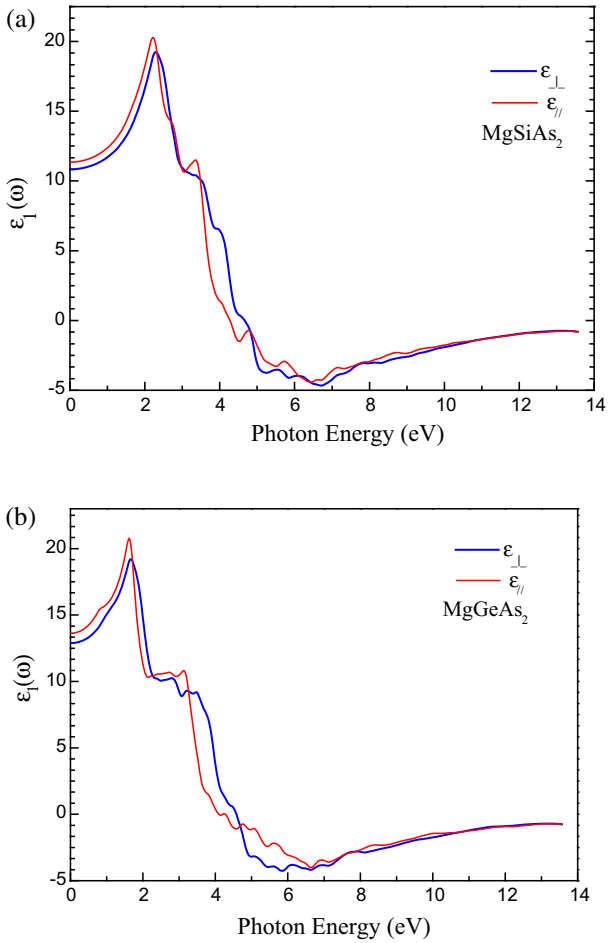

Figure 4. Calculated real $\varepsilon_1(\omega)$ parts of dielectric function for (**a**) $MgSiAs_2$ and (**b**) $MgGeAs_2$.

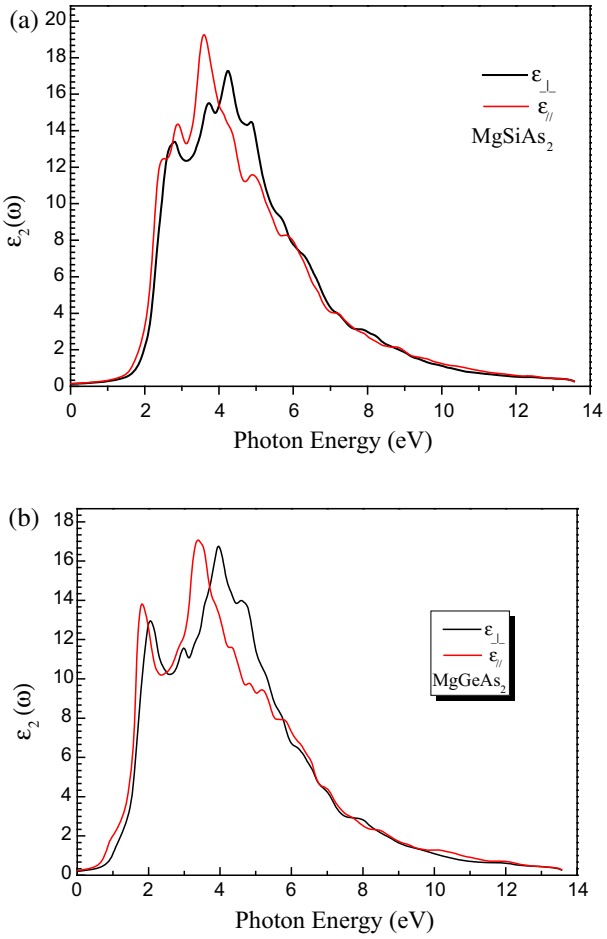

Figure 5. Calculated imaginary $\varepsilon_2(\omega)$ parts of dielectric function for (**a**) $MgSiAs_2$ and (**b**) $MgGeAs_2$.

The calculated static parallel and perpendicular components of the real dielectric function are given in table 3. We note that a smaller energy gap yields a larger $\varepsilon_1(0)$ value. This could be explained on the basis of the Penn model [22].

The imaginary part of the dielectric constant $\varepsilon_2(\omega)$ is displayed in figure 5. The main contributions to the optical spectra originate from the top valence bands to the lower conduction bands. The edge of the optical absorption in $MgSiAs_2$ and $MgGeAs_2$ occurs at about 1.2 eV and 0.6 eV, respectively. This position is the valence band and conduction band splitting at the Γ point ($\Gamma_v - \Gamma_c$) which gives the threshold for direct optical transition between the highest valence band and the lowest conduction band. This is known as the fundamental absorption edge. The obtained critical points are closely related to the obtained band-gap values. When a material is

Table 3. Calculated static real part of dielectric function, static refractive index $[n_\perp(0), n_\parallel(0)]$, static extinction coefficient $[K_\perp(0), K_\parallel(0)]$ and static birefringence $[\Delta n(0)]$ for $MgSiAs_2$ and $MgGeAs_2$.

	$\varepsilon_{1\perp}(0)$	$\varepsilon_{1\parallel}(0)$	$n_\perp(0)$	$n_\parallel(0)$	$\Delta n(0)$	$K_\perp(0)$	$K_\parallel(0)$
$MgSiAs_2$	8.96	9.01	2,93232	2,98687	0,08	0,00661	0,007
	9.121[a]	9.53[a]	3.020[a]	3.087[a]	0.046[b]		
$MgGeAs_2$	12.8	13.2	3,14695	3,2366	0,10	0,00865	0,00939
	10.208[a]	10.815[a]	3.195[a]	3.288[a]	0.093[a]		

[a]Ref. [10].
[b]Ref. [9].

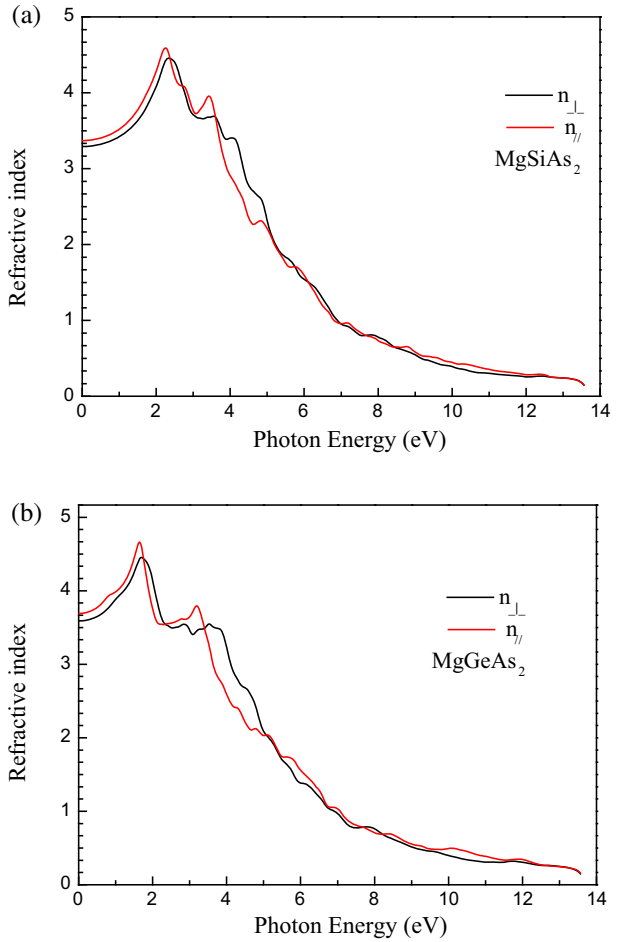

Figure 6. Calculated refractive index $n(\omega)$ for (**a**) $MgSiAs_2$ and (**b**) $MgGeAs_2$.

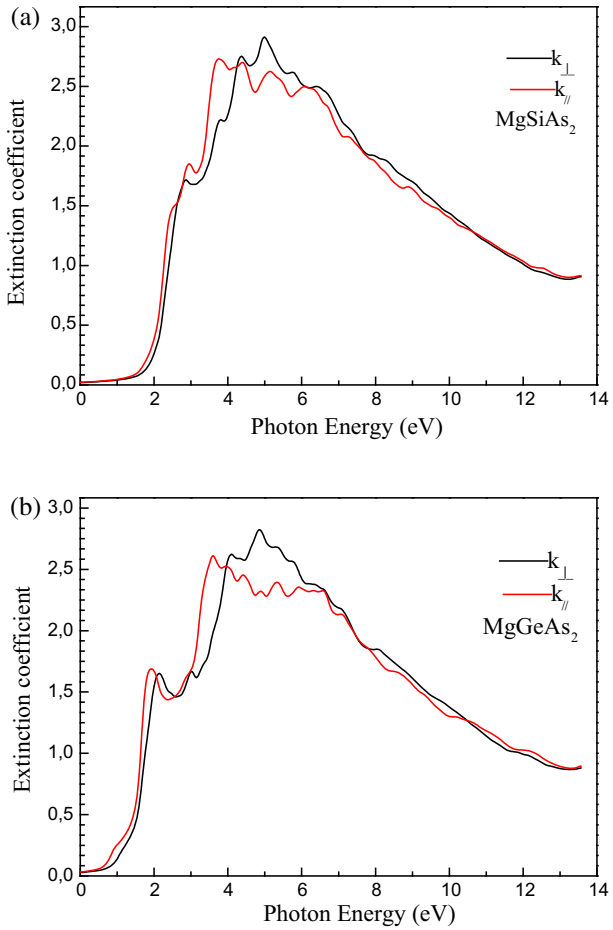

Figure 7. Calculated extinction coefficient $k(\omega)$ for (**a**) $MgSiAs_2$ and (**b**) $MgGeAs_2$.

transparent $\varepsilon_2(\omega)$ is zero, but it becomes non-zero when absorption begins.

The calculated refractive index is shown in figure 6. Uniaxial media have two main refractive indices: the extraordinary (parallel component of the refractive index noted as n_e) and ordinary (perpendicular component of the refractive index noted as n_0) refractive indices. The difference $\Delta n = n_e - n_0$ is then called birefringence of the medium. The refractive index spectrum shows an anisotropic behaviour ($\Delta n\,(0\,\text{eV}) = 0.08$ and 0.10 for $MgSiAs_2$ and $MgGeAs_2$, respectively). Beyond the zero frequency limits, the components n_0 and n_e increase with energy reaching a maximum value in the visible region for the two compounds and finally decrease with the further increase in energy. The obtained results for the static components of refractive index and birefringence are listed in table 3 along with the previously reported theoretical ones. The refractive index increases by changing Si to Ge.

The spectra of parallel ($k_\parallel$) and perpendicular ($k_\perp$) frequency-dependent extinction coefficient for the studied compounds are depicted in figure 7. The peak values obtained for the extinction coefficient occur at energies where the real part of the dielectric function $\varepsilon_1 = 0$. The static values for the extinction coefficient are given in table 3. The extinction coefficient decreases with increasing energy.

3.4 *Elastic properties*

The elastic constants C_{ij} determine the response of the crystal to external forces. They are among the most fundamental properties that can be predicted from the first-principle ground-state total energy calculations, and they are closely related to various fundamental solid-state phenomena such as interatomic bonding, equations of state, phonon spectra etc. For the tetragonal systems, there are six independent elastic constants ($M = 6$), namely, C_{11}, C_{12}, C_{13}, C_{33}, C_{44} and C_{66}. The determination of the elastic constants requires knowledge of the curvature of the energy curve as a function

Table 4. Calculated elastic constants (C_{ij}) (in GPa) of $MgSiAs_2$ and $MgGeAs_2$.

		This work	Other calculations
$MgSiAs_2$	C_{11}	95.3018	102.6[a]
	C_{12}	55.0016	42.6[a]
	C_{13}	54.3982	51.3[a]
	C_{33}	77.8709	69.100[a]
	C_{44}	66.0800	45.900[a]
	C_{66}	28.5222	42.3[a]
$MgGeAs_2$	C_{11}	80.127	83.834[b]
	C_{12}	53.142	42.475[b]
	C_{13}	48.801	46.107[b]
	C_{33}	71.367	66.439[b]
	C_{44}	34.851	29.789[b]
	C_{66}	29.964	34.701[b]

[a]Ref. [9].
[b]Ref. [23].

of strain for selected deformations of the unit cell. Deformations are chosen such that the strained systems have the maximum possible symmetry [23]. The WIEN2K package facilitates this task by providing a force-driven optimization of the internal cell geometry. The computed elastic moduli for $MgXAs_2$ (X = Si and Ge) compounds are listed in table 4. They are in reasonable agreement with the previously reported results. The requirement of mechanical stability in these systems leads to the following restrictions on the elastic constants:

$$C_{11} - C_{12} > 0, \quad C_{12} + C_{33} - 2C_{13} > 0,$$

$$2C_{11} + C_{33} + 2C_{12} - 4C_{13} > 0, \quad C_{11} > 0,$$

$$C_{33} > 0, \quad C_{44} > 0, \quad C_{66} > 0.$$

These criteria are satisfied, indicating that these compounds are mechanically stable.

3.5 *Thermal properties*

To investigate the thermal properties under high temperature and high pressure, we have applied the quasiharmonic Debye model as implemented in Gibbs program [24]. As a first step, a set of total energy calculation vs. primitive cell volume ($E - V$), in the static approximation, was carried out and fitted with a numerical EOS in order to determine its structural parameters at $P = 0$ and $T = 0$ and then derive the macroscopic properties as functions of P and T from standard thermodynamic relations. The thermal properties are determined in the temperature range from 0 to 1000 K and pressure range from 0 to 6.0 GPa.

Figure 8 displays the effect of temperature on the cell volume V at various pressures for the studied

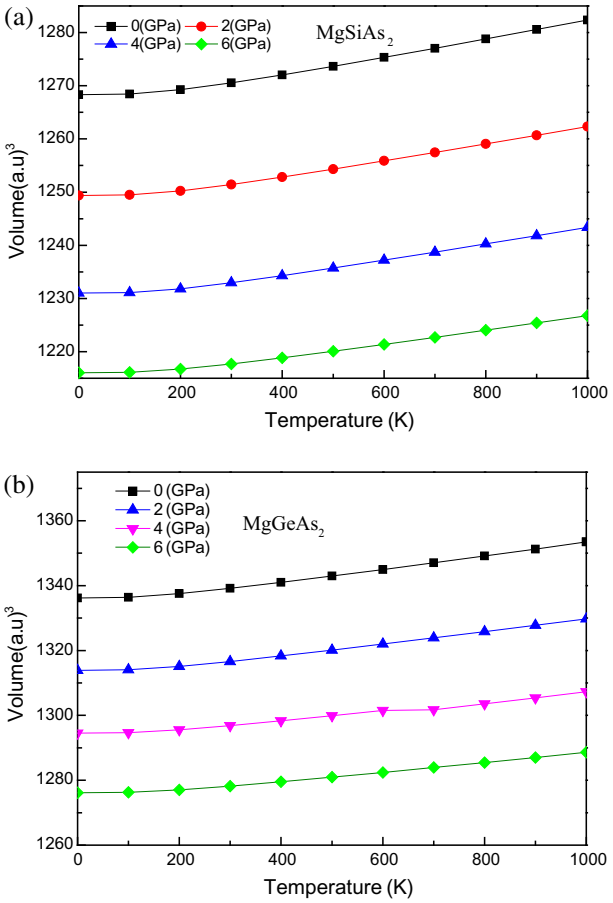

Figure 8. Variation of volume as a function of temperature under various pressures for (**a**) $MgSiAs_2$ and (**b**) $MgGeAs_2$.

compounds. The volume increases with increasing temperature at a given pressure. On the other hand, as the pressure increases the volume decreases at a given temperature but propensity of increment increases with temperature. The variation of bulk modulus vs. temperature at different pressures is shown in figure 9. The bulk modulus is nearly constant from 0 to 100 K and decreases when temperature is more than 100 K. The compressibility increases with increasing temperature at a given pressure and decreases with pressure at a given temperature. This indicates that the ability to resist the volume change becomes stronger when the pressure increases.

The Debye temperature θ_D is an important fundamental parameter closely related to many physical properties such as elastic constants, specific heat and melting temperature [25]. The dependence of the Debye temperature with pressure at various temperatures is plotted in figure 10. It can be seen that when the temperature is constant, the Debye temperature increases almost linearly with the increase of pressure. Furthermore, for a

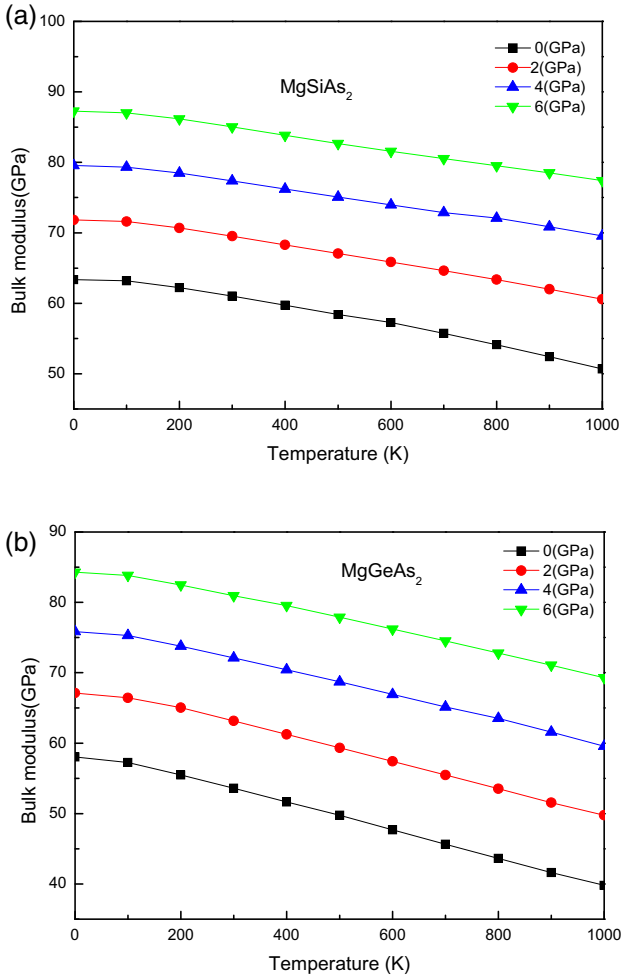

Figure 9. Variation of bulk modulus as a function of temperature under various pressures for (**a**) $MgSiAs_2$ and (**b**) $MgGeAs_2$.

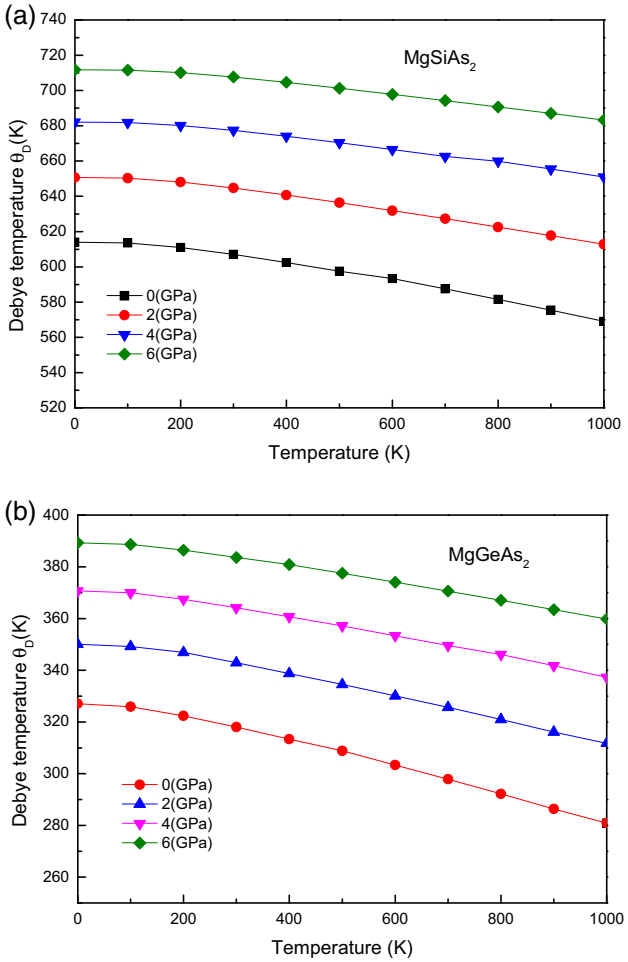

Figure 10. Variation of Debye temperature as a function of temperature under various pressures for (**a**) $MgSiAs_2$ and (**b**) $MgGeAs_2$.

given pressure, θ_D decreases with the increase of temperature. This result is in accordance with the fact that Debye temperature is proportional to the bulk modulus and that a hard material exhibits a high Debye temperature. Figure 11 displays the dependence of the thermal expansion coefficient α as a function of temperature and pressure. It can be seen that at a given pressure, α increases sharply at lower temperature (up to 300 K). When $T > 300$ K, α gradually approaches a linear increase with enhanced temperature and the propensity of increment becomes moderate, which means that the temperature dependence of α is very small at high temperature. In addition, with increasing pressure, α decreases sharply for a given temperature. At high temperatures and high pressures, the thermal expansion coefficient α would converge to a constant value.

Knowledge of heat capacity is mandatory for many applications, and so the variation of heat capacity at constant volume C_v vs. temperature at various pressures is shown in figure 12. The heat capacity at constant volume C_v increases sharply and is proportional to T^3 at low temperatures [26]. At high temperatures, the anharmonic effect on heat capacity is suppressed, and C_v tends to the Dulong–Petit limit [27]. It is noted that the effect of temperature on C_v is more significant than that of pressure. The initial increase in C_v with temperature under lower pressure is more rapid than under higher pressure.

4. Conclusions

The structural, electronic, optical, elastic and thermal properties of the chalcopyrites $MgSiAs_2$ and $MgGeAs_2$ have been investigated using FP-LAPW method based on DFT in combination with a quasiharmonic Debye

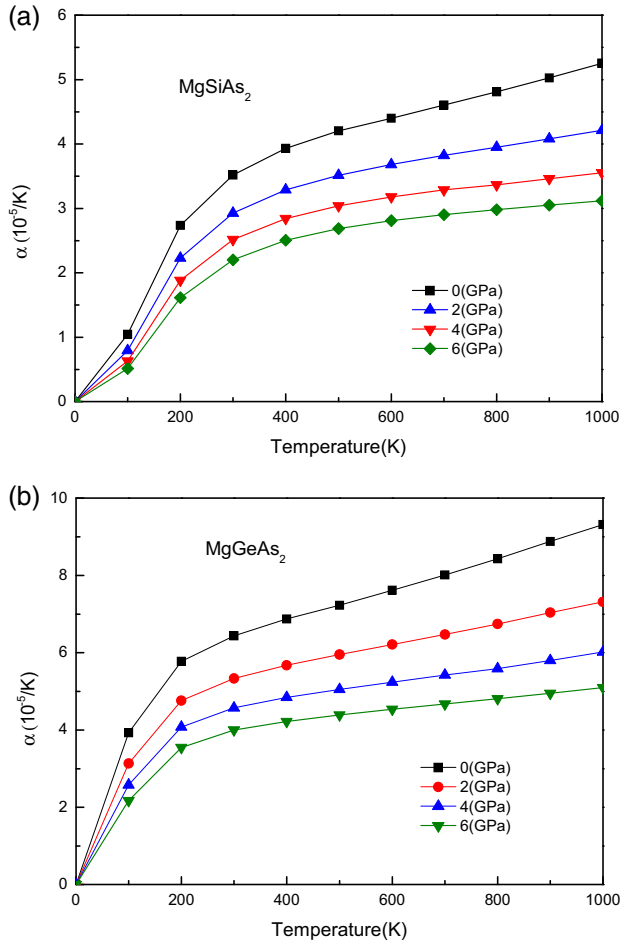

Figure 11. Variation of thermal expansion coefficient as a function of temperature under various pressures for (**a**) $MgSiAs_2$ and (**b**) $MgGeAs_2$.

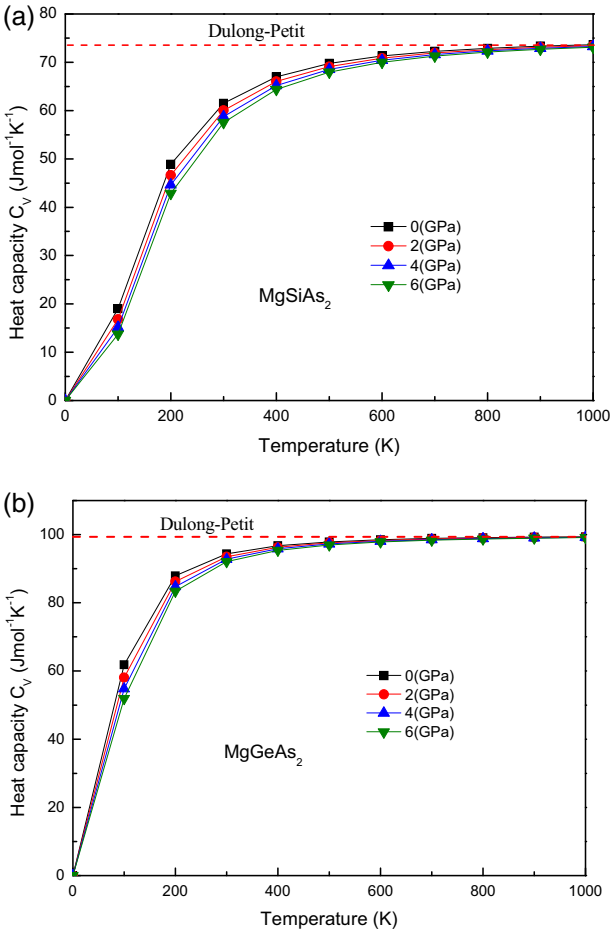

Figure 12. Variation of heat capacity C_v as a function of temperature under various pressures for (**a**) $MgSiAs_2$ and (**b**) $MgGeAs_2$.

model. A summary of the obtained results is as follows:

1. The calculated structural parameters are in good agreement with theoretical data.
2. These compounds are direct band-gap materials, the predicted band-gap values using mBJ scheme are significantly improved over the WC-GGA and are closer to the experimental findings.
3. The real and imaginary parts of the dielectric function, refractive index and extinction coefficient were determined. The static dielectric constants $\varepsilon(0)$ and static refractive index $n(0)$ have been calculated and a comparison has been made with the available theoretical values.
4. Thermal quantities such as thermal expansion coefficient, bulk modulus, heat capacity and Debye temperature are calculated successfully under various temperatures and pressures, and trends are discussed.

References

[1] F Chiker, Z Kebbab, R Miloua and N Benramdane, *Solid State Commun.* **151**, 1568 (2011)
[2] S Choi, G-B Cha, S Cho Hong, S Cho, Y Kim, J B Ketterson, S-Y Jeong and G-C Yi, *Solid State Commun.* **122**, 165 (2002)
[3] A V Kosobutsky, Yu M Basalaev and A S Poplavnoi, *Phys. Status Solidi B* **246**, 364 (2009)
[4] K C Bhamu, J Sahariya, R Vyas and K R Priolkar, *Pramana – J. Phys.* **89**, 1 (2017)
[5] J E Van Nostrand, J D Albrecht, R Cortez, K D Leedy, B Johnson and M J Oâkeefe, *J. Electron. Mater.* **34**, 1349 (2005)
[6] V L Shaposhnikov, A V Krivosheeva, V E Borisenko, J L Lazzari and F Arnaud d'Avitaya, *Phys. Rev. B* **85**, 20520 (2012)
[7] Liwei Shi, Jing Hu, Yun Qin, Yifeng Duan, Ling Wu, Xianqing Yang and Gang Tang, *J. Alloys Compounds* **611**, 210 (2014)
[8] Yu M Basalaev and P V Demushin, *J. Struct. Chem.* **51**, 1191 (2010)

[9] B Kocak and Y O Ciftci, *Mater. Res. Bull*. **77**, 300 (2016)
[10] F Boukabrine, F Chiker, R Miloua, Z Kebbab, R Khenata, Deo Prakash, S Bin Omran and K D Verma, *Opt. Mater*. **54**, 200 (2016)
[11] O K Anderson, *Phys. Rev. B* **42**, 3060 (1975)
[12] P Hohenberg and W Kohn, *Phys. Rev. B* **136**, 864 (1964)
[13] W Kohn and L S Sham, *Phys. Rev. A* **140**, 1133 (1965)
[14] P Blaha, K Schwarz, G K H Madsen, D Kvasnicka and J Luitz, wien2k. An augmented plane wave+ local orbitals program for calculating crystal properties, 2001
[15] Z Wu and R E Cohen, *Phys. Rev. B* **73**, 235116 (2006)
[16] F Tran and P Blaha, *Phys. Rev. Lett*. **102**, 226401 (2009)
[17] P E Blöchl, O Jepsen and O K Andersen, *Phys. Rev. B* **49**, 16223 (1994)
[18] F D Murnaghan, *Proc. Natl. Acad. Sci. USA* **30**, 5390 (1944)
[19] J E Jaffe and A Zunger, *Phys. Rev. B* **29**, 1882 (1984)
[20] Zh Zhaochun, P Ruiwu and C Nianyi, *Mater. Sci. Eng. B* **54**, 149 (1998)
[21] D J Singh, *Phys. Rev. B* **82**, 155145 (2010) D J Singh, *Phys. Rev. B* **82**, 205102 (2010)
[22] D R Penn, *Phys. Rev*. **128**, 2093 (1962)
[23] L Shi, J Hu, Y Qin, Y Duan, L Wu, X Yang and G Tang, *J. Alloys Compounds* **611**, 210 (2014)
[24] M A Blanco, E Francisco and V Luana, *Comput. Phys. Commun.* **158**, 57 (2004)
[25] V Kanchana, G Vaitheeswaran, A Svane and A Delin, *J. Phys.: Condens. Matter* **18**, 9615 (2006)
[26] P Debye, *Ann. Phys.* **344**, 789 (1912)
[27] A T Petit and P L Dulong, *Ann. Chim. Phys*. **10**, 395 (1819)